Chinese Chemical Letters 34 (2023) 107553

Contents lists available at ScienceDirect

Chinese Chemical Letters

journal homepage: www.elsevier.com/locate/cclet

Bifunctional separator with high thermal stability and lithium dendrite inhibition toward high safety lithium-ion batteries

Miaomiao Su[a], Yifu Chen[a], Suqing Wang[a,*], Haihui Wang[b,*]

[a] School of Chemistry & Chemical Engineering, South China University of Technology, Guangzhou 510640, China
[b] School of Chemical Engineering, Tsinghua University, Beijing 100084, China

ARTICLE INFO

Article history:
Received 19 April 2022
Revised 10 May 2022
Accepted 20 May 2022
Available online 23 May 2022

Keywords:
Separator
Lithium dendrite
Thermal stability
Halloysite nanotubes
Lithium-ion batteries

ABSTRACT

Coating inorganic ceramic particles on commercial polyolefin separators has been considered as an effective strategy to improve thermostability of separator. However, the introduction of the coating layer could induce pore blockage on the surface of the polyolefin separator. Herein, a ceramic composite layer that consists of alumina nanoparticles (n-Al_2O_3) and halloysite nanotubes (HNTs) is designed to modify the polyethylene (PE) separator (the modified separator is denoted as AH-PE). The HNTs with hollow nanotubular structure construct a light skeleton and provide fast ion transport channels while Al_2O_3 particles function as heat-resistant fillers to inhibit the shrinkage of the separator at elevated temperatures. The total thickness of AH-PE separator is only 14 μm. Consequently, the mass increment of AH-PE separator decreases from 5 g/m^2 to 3.5 g/m^2, and the Gurley value reduces by 23%, compared with Al_2O_3 coated PE separator (A-PE). Due to the synergistic effects of Al_2O_3 and HNTs, AH-PE separator exhibits highly improved thermal stability (almost no shrinkage at 170 °C for 30 min), high Li^+ transference number (up to 0.47), and long cycle life of 450 h for Li|Li cells. Moreover, the $LiFePO_4$/Li cells assembled with AH-PE separators demonstrate improved rate capability and safety performance.

Owing to high energy density and long cycle life, lithium-ion batteries (LIBs) have been widely adopted in various applications, such as electric vehicles, laptops and digital cameras. However, the increasing energy density of LIBs has made their safety issues become a critical concern. Different strategies have been deployed to increase the reliability of LIBs. Within all these strategies, separator, as a key component in LIBs which enables lithium ions transportation inside the battery and avoids the direct contact of the electrodes, plays a crucial role regarding safety of batteries [1–3]. However, current commercial polyolefin separators with low melting points easily shrink at elevated temperatures, leading to internal short circuit and even explosion [4–7].

Developing heat-resistant separators is a common method to improve the safety of batteries [8–11]. For large scale production, coating ceramic heat-resistant materials, such as Al_2O_3, silica (SiO_2), and boehmite (AlOOH) on one or both sides of the polyolefin separators have been proven to be an effective strategy to enhance the thermostability of separators due to the low-cost and processability of the materials [12–20]. Specifically, ceramic coated separators exhibited highly improved thermal stability and electrolyte uptake, but they were still subject to some inherent limitations, such as pores blockage, increasing mass loading and total thickness [21–24]. In addition, thickening of the coating layer inevitably prolongs path for ion transport and further affects air permeability of separators [25–27]. The air permeability represented by the Gurley value (s/100 mL), evaluating by measuring the time for air to pass through a certain volume (100 mL). Typically, a low Gurley value indicates high air permeability. Lee *et al.* designed a multilayer-coated separator (MCS) containing Al_2O_3 coating layer and adhesive coating layer [21]. The Gurley value increased from 171 s/100 mL to 284 s/100 mL for MCS. Apart from thermal stability, dendrite-inhibited is also very important for separator safety which is closely related to the mechanical strength and the uniform lithium ions transport performance of the separators. Halloysite nanotube (HNT, $Al_2Si_2O_5(OH)_4{\cdot}2H_2O$) is a natural clay composed of nanosized tubular aluminosilicate layers [28–31]. As polar functional groups, Si–O tetrahedron on the outer surface and Al–O octahedron on the inner surface, resulting in the negatively (out) and positively (inner) charge surfaces of HNT, which facilitates the dissociation of the Li salts, thus benefit the Li^+ migration through HNT. In addition, the differences in HNTs surface charge have also been exploited for ion shielding functional separator for lithium-

* Corresponding authors.
E-mail addresses: cesqwang@scut.edu.cn (S. Wang), cesqwang@scut.edu.cn (H. Wang).

https://doi.org/10.1016/j.cclet.2022.05.067
1001-8417/

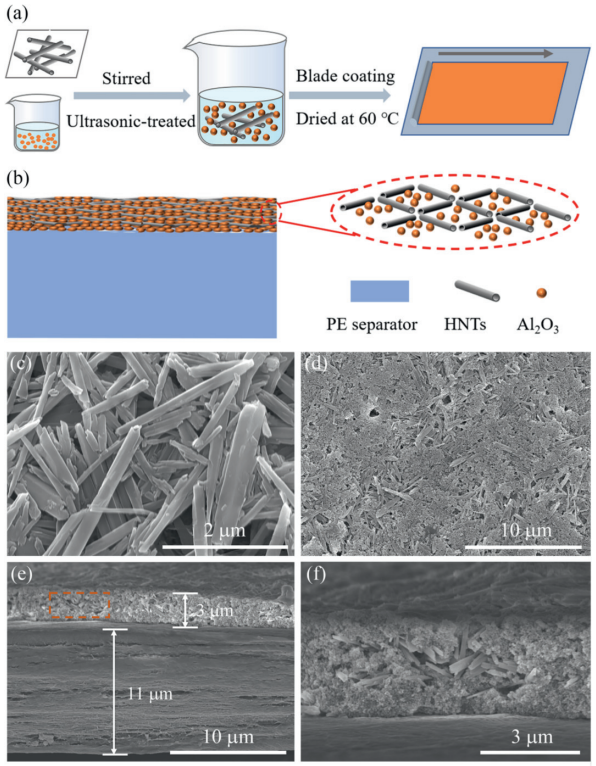

Fig. 1. Schematic illustration of (a) the preparation process of the AH-PE separator and (b) cross-section of the coating layer. (c) SEM image of pure HNTs. (d) Surface and (e) cross-sectional SEM images of AH-PE separator. (f) Enlarged cross-sectional SEM image of the modified layer.

sulfur batteries [29]. It was also reported that the surface coating with HNT on separator or Li metal anode could prevent lithium dendrites from piercing the separator and then improve the stability of lithium-ion batteries [30,31]. Xie developed a novel separator with coating HNTs on both sides of a 25 μm polypropylene (PP) separator [30]. The rich pore structure and sufficient surface hydroxyl groups can enhance electrolyte wettability and absorption, the thermal stability of the separator was also enhanced. However, the total thickness of coating layers was around 10 μm which highly affect the energy density of the battery. Therefore, it is necessary to optimize the coating layer to achieve stable thermal stability and high dendrite-inhibited performance without sacrificing intrinsic excellent electrochemical properties of separators.

In this study, a coating layer with dual-pore structure consisting of two different sizes of inorganic materials (Al_2O_3 nanoparticles and halloysite nanotubes) is designed to modify the PE separator (denoted as AH-PE). The halloysite nanotubes act as light skeleton hierarchy and provide sufficient ion transport channels while nano-sized alumina particles fill empty space of the matrix to form a tightly stacked coating. In addition, the positively charge at inner surfaces of HNTs could restrict the migration of anions and facilitate transportation of lithium ions. Due to the synergistic effects of Al_2O_3 and HNTs, AH-PE separator with a total thickness of 14 μm exhibits better thermal stability, higher ionic conductivity and higher Li^+ transference number than pristine PE separator. The $LiFePO_4$/Li cells assembled with AH-PE separators show exceptional rate capability and safety performance.

The preparation process of the AH-PE separator was illustrated in Figs. 1a and b, the Al_2O_3 nanoparticles and HNTs were mixed with lithium polyacrylate (PAALi) as binder in water to obtain the coating slurry, and then the AH-PE was prepared by blading the mixed slurry onto one side of the PE separator. Compared with organic slurry using toxic organic solvents tends which pollute the environment and the increase cost of organic solvent recovery, the use of water-based ceramic slurry is environmentally friendly. Fig. 1c and Fig. S1a (Supporting information) showed the typical hallow tubular morphology of HNTs. Fig. S1b (Supporting information) indicated that HNTs possess abundant surface inside or outside of tube with a high BET specific surface area of 25.7 m^2/g. Besides, according to the result of the pore size distribution, HNTs have a wide range 2–20 nm of the inner diameter, obviously peaks appeared at 3 nm and 12 nm, which corresponded to the halloysite surface pore (crystallization defect location) and the inner diameter of tube, respectively. Appropriate inner diameter of HNTs not only provide additional channels for Li^+ transport but also uniformly distribute Li ionic flux. According to the statistical results (Figs. S2a and b in Supporting information), HNTs exhibited length of 450–2550 nm and outer diameter of 70–190 nm with aspect ratio of 2–36. The large aspect ratio of HNTs could construct skeleton hierarchy and Al_2O_3 nanoparticles evenly fill the gaps, forming three-dimension porous coating.

From the surface SEM image of AH-PE separator in Fig. 1d, Al_2O_3 and HNTs were homogeneously distributed with small pores. To better explain the dual-pore structure, the cross-sectional morphology of AH-PE separator was investigated (Figs. 1e and f). The thickness of the tightly packed composite coating layer is approximately 3.0 μm. Enlarged image suggested that the embedded HNTs with hallow structure provide additional pores for ionic migration. Meanwhile, the well-connected interstitial voids between Al_2O_3 nanoparticles and HNTs also formed the three-dimension porous structure. For comparison, the H-PE separator coated with pure HNTs showed porous coating structure due to the loose stack of HNTs (Figs. S3a and b in Supporting information). In contrast, the A-PE separator coated with single Al_2O_3 showed severe cracks on the surface due to the agglomerated and unevenly distributed Al_2O_3 nanoparticles (Figs. S4a-c in Supporting information). The SEM elemental mapping images of AH-PE separator in Figs. S5a-d (Supporting information) suggested the matched spatial distribution of C, Si and Al, further confirming the uniform distribution of Al_2O_3 and HNTs. The XRD patterns of HNTs powders, AH-PE and PE separators were shown in Fig. S6 (Supporting information). In the case of AH-PE separator, peaks appeared at 21.5° and 23.9° corresponding to PE, and the peak at 12° was indexed to HNTs. Meanwhile, the density of HNTs (2.6 g/cm^3) is lower than commercial Al_2O_3 particles (4.0 g/cm^3), so the introduction of HNTs effectively reduced the mass loading of coating layer, the mass increment decreased from 5 g/m^2 for A-PE separator to 3.5 g/m^2 for AH-PE separator.

The permeability of separator was characterized by air permeability measurement, represented by the Gurley value. As shown in Fig. 2a, the Gurley values of H-PE, A-PE and AH-PE separators were 159, 256 and 197 s/100 mL, respectively. H-PE and AH-PE separators showed lower Gurley values than that of A-PE separator, indicating that the introduction of hollow HNTs could help to provide fast ion transport channels. In addition to air permeability, separator is also required to possess adequate mechanical strength to meet the needs of cell assembly. As shown in Fig. 2b, the tensile strengths of A-PE and AH-PE separators were all approximately 170 MPa, which were slightly higher than that of the PE separator (161 MPa). The strain values of A-PE (73.6%) and AH-PE (76.6%) were significantly higher than that of PE separator (52.7%) due to the strong adhesive force between the tight coating and the PE substrate. The loose structure of the coating layer in H-PE separator may weaken the adhesion with PE substrate, and the strain value of H-PE separator was similar with that of PE separator. Compared with A-PE separator, the improved mechanical property of AH-PE separator might ascribe to the introduction of HNTs which helped to reduce the agglomeration of Al_2O_3 nanoparticles and contributed to the forma-

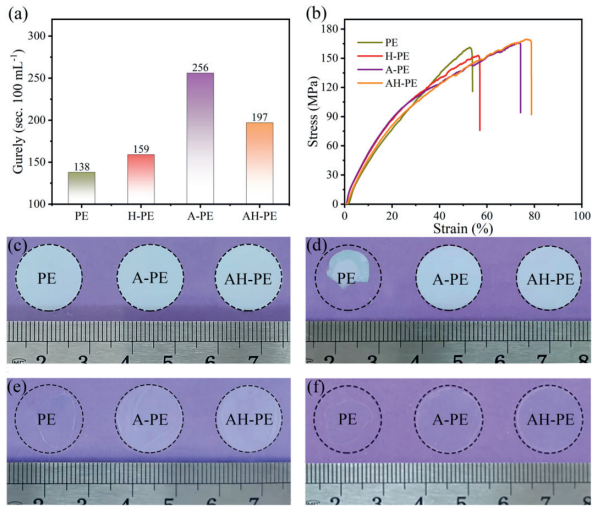

Fig. 2. (a) Gurley values and (b) tensile stress-strain curves of different separators. Thermal shrinkage of bare PE, A-PE and AH-PE separators: (c) at 30 °C, after thermal treatment at (d) 150 °C, (e) 160 °C, and (f) 170 °C for 0.5 h.

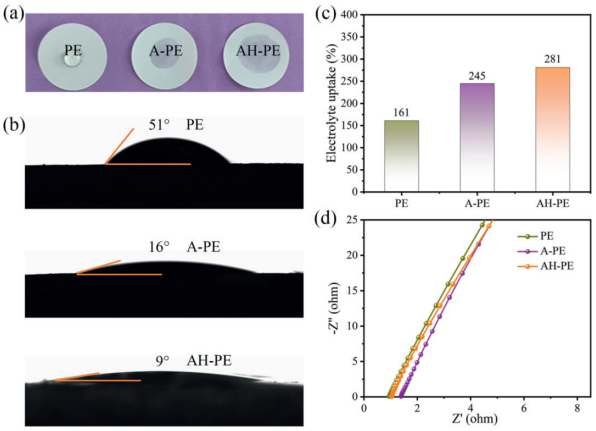

Fig. 3. (a) Photographs of wetting behavior, (b) electrolyte contact angles, and (c) electrolyte uptakes of separators. (d) The EIS spectra of SS/separator/SS cells using PE, A-PE and AH-PE separators, respectively.

tion of a more uniform coating. To investigate the thermal stability, the separators were kept in the oven at different temperatures for 0.5 h. The photographs of the PE, H-PE, A-PE and AH-PE separators before and after heat treatment at 140 °C were shown in Figs. S7a and b (Supporting information). Both PE and H-PE separators could not maintain its original shape with large thermal shrinkages while the A-PE and AH-PE separators kept stable. Compared with the original shape before heat treatment (Fig. 2c), when further increasing the test temperature, the A-PE and AH-PE separators showed no shrinkage below 160 °C (Figs. 2d and e), and exhibited less than 5% thermal shrinkage at 170 °C (Fig. 2f). Fig. S8 (Supporting information) indicated that the surface morphology of AH-PE separator remained largely unchanged after heat treatment at 160 °C for 0.5 h. Owing to the strong adhesion between the coating and the PE substrate, the modified separator could maintain the original dimension even though the PE separator melted at elevated temperature.

Wettability of separator with liquid electrolyte is a vital factor influencing the battery performance. As shown in Figs. 3a and b, large contact angle (51°) was measured on the pristine PE separator indicating poor wettability of polyolefin separator, while the electrolyte spread out rapidly for A-PE and AH-PE separators with lower contact angels. Such an improved electrolyte wettability of

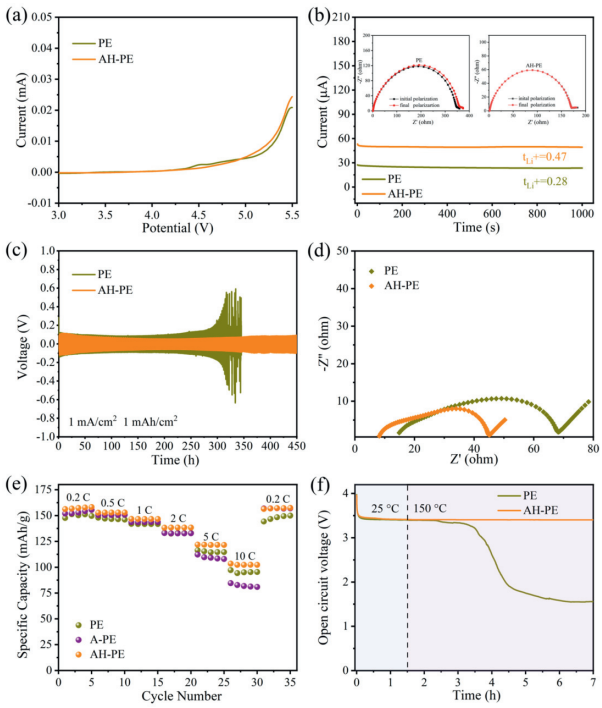

Fig. 4. (a) LSV curves of the cells using different separators. (b) Chronoamperometry of Li/electrolyte-soaked separator/Li cells (the inset showed the corresponding EIS curves before and after polarization). (c) Galvanostatic cycling properties of symmetric Li/Li cells at 1 mA/cm^2 with a fixed capacity of 1 mAh/cm^2. (d) Comparison of EIS spectra of Li/Li cells using different separators after cycling 200 h. (e) Rate capability of $LiFePO_4$/Li cells using different separators. (f) The open circuit voltages of the $LiFePO_4$/Li cells assembled with PE and AH-PE separators at 150 °C.

AH-PE separator should be attributed to the abundant hydroxyl groups on the surface of both Al_2O_3 and HNTs. The sufficient polar functional groups enhanced the affinity for polar electrolyte. The electrolyte uptake results in Fig. 3c further illustrated the affinity of porous coating to electrolyte. The electrolyte uptake of A-PE, AH-PE separators were 245%, 281% respectively, which were higher than that of PE separator (161%). EIS curves were measured *via* sandwiching the electrolyte-soaked separators between two SS electrodes to evaluate the ionic conductivity (Fig. 3d). The ionic conductivity of AH-PE separator was calculated to be 0.67 mS/cm which was higher than that of the PE (0.58 mS/cm) and A-PE separator (0.51 mS/cm). The increasing ionic conductivity suggested that the dual-pore coating structure could provide abundant channels for the efficient migration of Li ions. Meanwhile, the positive charge distributed on the inner surface of halloysite nanotubes could adsorb anions in the electrolyte and accelerate more Li ions movement [30]. The relatively poor ionic conductivity of A-PE separator also indirectly confirmed the critical role of halloysite nanotubes in improving the Li-ion conductivity.

The LSV measurement was conducted to test the electrochemical stability of different separators. As shown in Fig. 4a, the cell using AH-PE separator exhibited a stable electrochemical operating window (~4.6 V), illustrated that there was no side reaction between separator and electrolyte or lithium mental. In addition to the better electrochemical stability, the AH-PE separator also offered a relatively higher Li^+ ion transference number (t_{Li^+}). As shown in Fig. 4b, the t_{Li^+} was improved from 0.28 for PE separator to 0.47 for AH-PE separator, which was mainly attributed to the trapping effects of electrolyte anions by HNT. The oppositely charged surfaces of HNT facilitated dissociation the lithium salt. Specifically, the anions were adsorbed by the positive charge on the inner surface of the HNTs and immobilized within the

tube channels [31]. Therefore, more free lithium ions can migrate through the internal channels of the tubes [32]. The galvanostatic cycling of symmetrical Li|Li cells at 1 mA/cm^2 with a fixed capacity of 1 mAh/cm^2 was conducted to further evaluate the long-term cycling stability. As shown in Fig. 4c and Figs. S9a-c (Supporting information), the pristine PE separator exhibited quick growth in voltage hysteresis after 300 h and a sudden voltage drop occurred around 320 h due to short circuit induced by lithium dendrites. Interestingly, AH-PE separator showed stable voltage profiles with an average overpotential of about 87 mV for 450 h. We further characterized the surface morphologies of lithium metal anodes from cells assembling with different separators after 300 h cycling. As shown in Figs. S10a and b (Supporting information), the lithium metal anode with AH-PE separator had a more uniform and dense lithium deposition surface than that assembled with PE separator. These results illustrated that the enhanced electrolyte wettability of AH-PE separator and the abundant transport channels provided by the dual-pore structure all promoted fast and uniform transmission of lithium ions, suppressing the growth of lithium dendrite, facilitating the formation of uniform and dense Li deposition layer. Fig. 4d showed the AC impedance spectra of Li/Li cells using different separators after 200 h cycling process. The results further revealed that cell assembled with AH-PE separator exhibited a lower interfacial impedance than that with the PE separator.

Furthermore, the rate capability of cells was depicted in Fig. 4e. The cells using PE, A-PE and AH-PE separators delivered capacities of 147.7 mAh/g, 152 mAh/g, 156.3 mAh/g at 0.2 C, respectively. At elevated current densities, the cell with AH-PE separator exhibited higher discharge capacities than the cells using PE and A-PE separators, delivered capacities of 146.8 mAh/g, 138.3 mAh/g, 121.9 mAh/g, 103.5 mAh/g at 1, 2, 5 and 10 C, respectively. The battery cycling stability was further studied and showed in Fig. S11 (Supporting information). The three cells exhibited the same discharge capacity at first. After 200 cycles, the discharge capacity of the cell assembled with AH-PE separator was 130.3 mAh/g, higher than that of using PE separator (124.5 mAh/g) and A-PE separator (124.6 mAh/g). The superior rate capability and cycling performance of the cells using AH-PE separators were attributed to the dual pore structure and improved wettability property, which facilitated the transport of lithium ions between the separator and the electrode. In addition, we analyzed the stability of the Al_2O_3/HNTs coating layer after cycling. From the surface and cross-sectional SEM images of the cycled AH-PE (Figs. S12a and b in Supporting information), we could find that the coating layer was stable and did not fall off from the PE substrate, illustrating the good structure stability of AH-PE separator.

In order to further evaluate the safety performance of batteries, cells with different separators were charged to 4.0 V, and then variation of open circuit voltage (OCV) of cells at 150 °C were measured as a function of storage time. As shown in Fig. 4f, the cell assembled with PE separator experienced an obvious voltage disturbance when the temperature reached to 150 °C and the OCV suddenly dropped within 3.5 h due to the thermal shrinkage of the separator, while the cell using AH-PE separator could still hold ~3.40 V after the same experiment, indicating that the dimensional stability of the AH-PE separator at high temperature could help to avoid internal short-circuiting of cell, ensuring high safety of lithium-ion batteries.

In summary, a bifunctional separator with high thermal stability and lithium dendrite inhibition was successfully fabricated. The dual-pore structure of the coating layer provided abundant channels to regulate homogenous Li migration and deposition. Compared with A-PE separator, AH-PE separator with the uniform porous structure exhibited lower mass loading, better air permeability, higher ionic conductivity and Li^+ transference number. As a result, the cells with AH-PE separators exhibited fascinating lifespan with low overpotential (87 mV after 450 h) as well as the remarkable thermal stability (almost no shrinkage at 170 °C). More importantly, the $LiFePO_4$/Li cells assembled with AH-PE separators showed improved rate capability and safety performance. This work provides a viable path for the further development of separators for safety lithium ions batteries.

Declaration of competing interest

The authors declare that they have no known competing financial interests or personal relationships that could have appeared to influence the work reported in this paper.

Acknowledgments

This work was supported by the National Natural Science Foundation of China (No. 22178120), the Guangdong Natural Science Funds for Distinguished Young Scholar (No. 2017A030306022) and Guangzhou Technology Project (No. 202002030164).

Supplementary materials

Supplementary material associated with this article can be found, in the online version, at doi:10.1016/j.cclet.2022.05.067.

References

[1] X. Huang, R. He, M. Li, et al., Mater. Today 41 (2020) 143–155.
[2] M. Su, G. Huang, S. Wang, Y. Wang, H. Wang, Sci. China Chem. 64 (2021) 1131–1156.
[3] Y. Wang, S. Wang, J. Fang, L. Ding, H. Wang, J. Membr. Sci. 537 (2017) 248–254.
[4] X. Feng, D. Ren, X. He, M. Ouyang, Joule 4 (2020) 743–770.
[5] X. Qiu, Z. Li, X. Li, Z. Zhang, Chem. Eng. J. 334 (2018) 108–122.
[6] K. Liu, Y. Liu, D. Lin, A. Pei, Y. Cui, Sci. Adv. 4 (2018) 9809–9820.
[7] Q. Wang, B. Mao, S.I. Stoliarov, J. Sun, Prog. Energy Combust. Sci. 73 (2019) 95–131.
[8] T. Dong, W.U. Arifeen, J. Choi, K. Yoo, T. Ko, Chem. Eng. J. 398 (2020) 125646.
[9] H. Zhao, N. Deng, J. Yan, et al., Chem. Eng. J. 356 (2019) 11–21.
[10] Y. Zhang, Z. Wang, H. Xiang, P. Shi, H. Wang, J. Membr. Sci. 509 (2016) 19–26.
[11] J. Liang, Q. Chen, X. Liao, et al., Angew. Chem. Int. Ed. 59 (2020) 6561–6566.
[12] Z. Wang, H. Xiang, L. Wang, et al., J. Membr. Sci. 553 (2018) 10–16.
[13] J. Chen, S. Wang, D. Cai, H. Wang, J. Membr. Sci. 449 (2014) 169–175.
[14] C. Yang, H. Tong, C. Luo, et al., J. Power Sources 348 (2017) 80–86.
[15] M. Waqas, S. Ali, C. Feng, et al., Small 15 (2019) 1901689.
[16] Y. Yang, W. Wang, J. Zhang, Mater. Today Energy 16 (2020) 100420.
[17] M.J. Uddin, P.K. Alaboina, L. Zhang, S.J. Cho, Mater. Sci. Eng. B 223 (2017) 84–90.
[18] J.H. Ahn, H.M. Kim, Y.J. Lee, et al., J. Power Sources 506 (2021) 230119–230130.
[19] H. Jeon, D. Yeon, T. Lee, et al., J. Power Sources 315 (2016) 161–168.
[20] R. Xu, L. Sheng, H. Gong, et al., Adv. Eng. Mater. 23 (2021) 2001009–2001016.
[21] S.H. Lee, J. Kim, B.H. Kim, S. Yoon, K.Y. Cho, Small 15 (2019) 1804980.
[22] Y. Li, L. Yu, W. Hu, X. Hu, J. Mater. Chem. A (2020) 20294–20317.
[23] X. Qi, Z. Zhang, C. Tu, et al., Appl. Surf. Sci. 541 (2021) 148405.
[24] W.K. Shin, D.W. Kim, J. Power Sources 226 (2013) 54–60.
[25] B. Jung, B. Lee, Y.C. Jeong, et al., J. Power Sources 427 (2019) 271–282.
[26] L. Yu, Y. Jin, Y.S. Lin, RSC Adv. 6 (2016) 40002–40009.
[27] W. Chen, L. Shi, H. Zhou, et al., ACS Sustain. Chem. Eng. 4 (2016) 3794–3802.
[28] C. Huang, H. Ji, B. Guo, et al., Cellulose 26 (2019) 6669–6681.
[29] Y.M. Kwon, J. Kim, K.Y. Cho, S. Yoon, J. Energy Chem. 60 (2021) 334–340.
[30] Y. Xie, X. Chen, K. Han, X. Xiong, Electrochim. Acta 379 (2021) 138182.
[31] H. Liu, R. Tao, C. Guo, et al., Chem. Eng. J. 429 (2022) 132239.
[32] J. Feng, X. Ao, Z. Lei, et al., Electrochim. Acta 340 (2020) 135995.